Analytical approaches to describe the near source effects

Sarva Jit Singh
Department of Mathematics, Maharshi Dayanand University, Rohtak 124 001, India

The application of dislocation models for earthquake faulting has become routine in the present-day studies of the dynamic field induced by earthquakes. In this review article, we discuss the effect of the finiteness of a dislocation source and its motion on body wave radiation patterns. The Aki-Haskell model used for computing the near-field ground motion is also described.

The mathematical foundation for the calculation of the near field ground motion was laid[1, 2] in the early 1960s when it was shown that the point-force equivalent of fault-slip is a double couple and that the seismogram can be synthesized by a space-time convolution of the slip function and a Green's function. The slip function describes the fault displacement during an earthquake as a function of time and position on the fault plane. Green's function is the response of the earth when an impulsive double couple is applied at a point on the fault plane. The slip function and Green's function express quantitatively the source and propagation effects, respectively, on seismic motion.

A number of theoretical studies have been undertaken during the last quarter of a century to calculate the near-field ground motion. The earliest works[3, 4] are based on the results of Maruyama[1] and Burridge and Knopoff[2] on dislocation sources in an unbounded medium. The effect of the free surface was later incorporated[5]. The response of a horizontally layered crustal structure has been calculated by various analytical techniques[6].

Body waves from a finite moving dislocation

The sources of seismic waves in the earth are not always localized in time and space. It is well known that the fracture zones in cases of major earthquakes may be as long as 700 km. Moreover, in general, the rupture propagates along the fault with an average velocity of 3 to 3.5 km/s. To account for the observed radiation field from such sources, suitable models are necessary which take into account the finiteness of the source and its motion. The simplest way is to start with the expression for the far-field of a point dislocation source and integrate over the fault with proper time delays so as to simulate a source moving with a uniform velocity[7-9].

The *P*-wave displacement in the far-field due to an arbitrary shear dislocation may be expressed in the form[10]

$$u^P = \frac{\mathrm{d}S}{12\pi\beta}\,(\beta/\alpha)^3\,F\,\dot{U}\left(t-\frac{R}{\alpha}\right)\frac{1}{R}\,, \qquad (1)$$

where $\mathrm{d}S$ = fault area, α = *P*-wave velocity, β = *S*-wave velocity, F = radiation pattern function, R = source-receiver distance, and $\dot{U}(t) = \mathrm{d}U/\mathrm{d}t$ = slip velocity.

Let us consider a rectangular fault of length L and width W (Figure 1). We assume that the rupture initiates simultaneously along the entire width of one end of the fault and propagates along its length with a constant *rupture velocity* V. We also assume that the dislocation (slip) U is a function of time and space of the form $U(s, t)$, where s is the distance measured along the length of the fault. For a finite moving dislocation, equation (1) becomes

$$u^P = \frac{W}{12\pi\beta}\,(\beta/\alpha)^3\,F \int_0^L \dot{U}\left(s;\, t-\frac{S}{V}-\frac{R}{\alpha}\right)\frac{1}{R}\,\mathrm{d}s\,, \qquad (2)$$

assuming W/L to be small (Figure 2). In equation (2), t has been replaced by $t-s/V$ to include the finite velocity of rupture.

Let R_0 be the distance of the receiver P from the corner Q of the rupturing end of the fault. Assuming

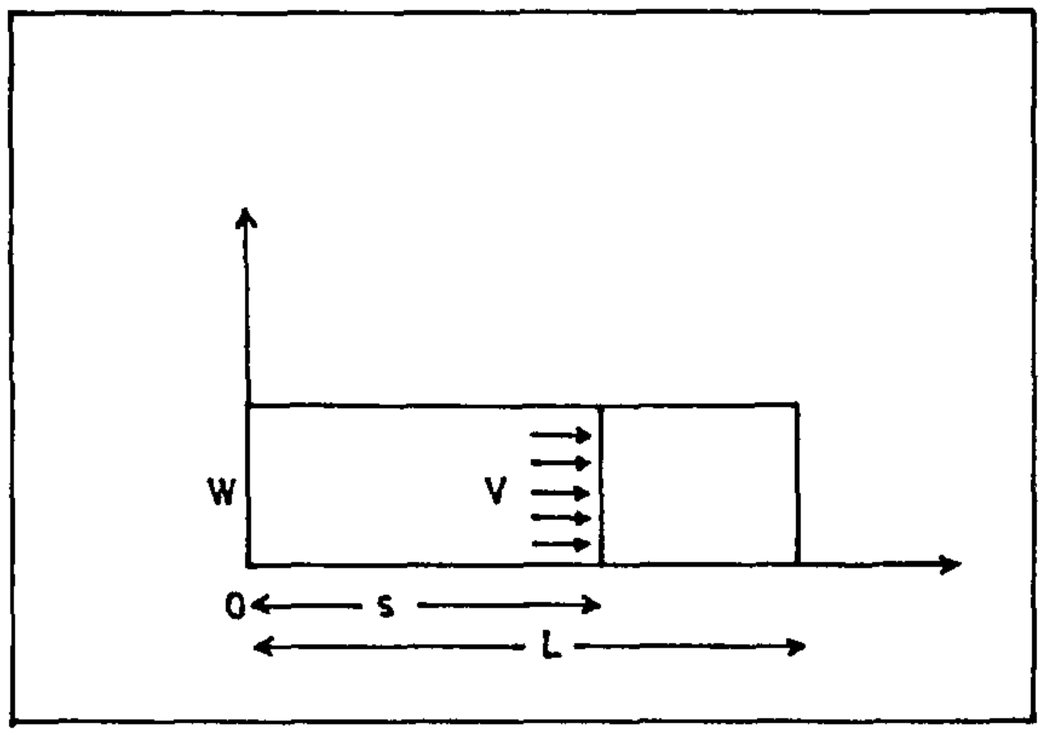

Figure 1. Unidirectional faulting on a rectangular fault

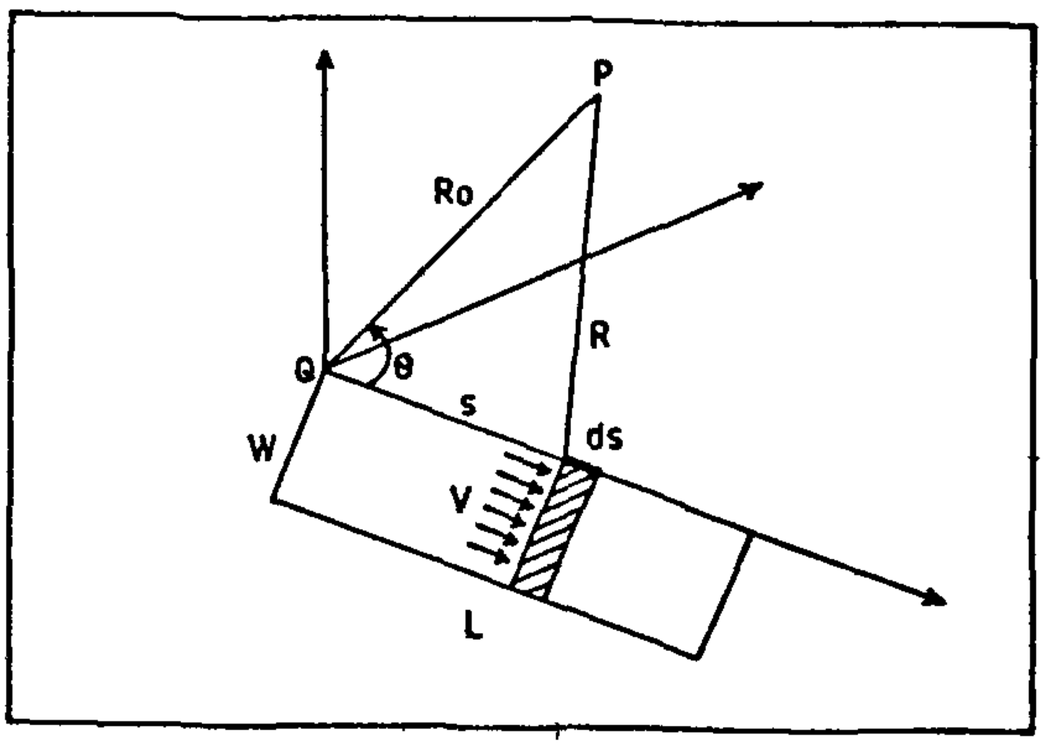

Figure 2. The geometry of a finite moving dislocation.

$R_0 \gg s$, we have (Figure 2)

$$R = (R_0^2 - 2R_0 s \cos\theta + s^2)^{1/2}$$

$$\simeq R_0 - s \cos\theta,$$

where θ is the angle between the direction to the receiver P from Q and the direction of rupture propagation. Equation (2) now becomes

$$u^P = \frac{W}{12\pi\beta} (\beta/\alpha)^3 \frac{F}{R_0} \int_0^L \dot{U}\left[s; t - \frac{R_0}{\alpha} - \frac{s}{V}\left(1 - \frac{V}{\alpha}\cos\theta\right)\right] ds. \quad (3)$$

Assuming $U(s, t) = U_0 g(t)$, we have

$$\dot{U}\left[s; t - \frac{R_0}{\alpha} - \frac{s}{V}\left(1 - \frac{V}{\alpha}\cos\theta\right)\right]$$

$$= U_0 \dot{g}\left[t - \frac{R_0}{\alpha} - \frac{s}{V}\left(1 - \frac{V}{\alpha}\cos\theta\right)\right]$$

$$= -\frac{VU_0}{1 - (V/\alpha)\cos\theta}$$

$$\frac{\partial}{\partial s} g\left[t - \frac{R_0}{\alpha} - \frac{s}{V}\left(1 - \frac{V}{\alpha}\cos\theta\right)\right]. \quad (4)$$

Equations (3) and (4) yield

$$u^P = \frac{P_0}{12\pi\beta} (\beta/\alpha)^3 \frac{F}{R_0}\left[\frac{g(t_\alpha) - g(t_\alpha - t_d^\alpha)}{t_d^\alpha}\right], \quad (5)$$

where $P_0 = U_0 LW$ = source-potency and

$$t_\alpha = t - R_0/\alpha,\ t_d^\alpha = \frac{L}{V}\left(1 - \frac{V}{\alpha}\cos\theta\right).$$

Comparing equations (1) and (5), we note that the field due to a moving dislocation along a finite fault can be interpreted as the difference of the fields of two point dislocations located at Q, which start radiating at an interval of t_d^α. The entity t_d^α is the duration of the P signal at the observation point. Similarly, the duration of the S signal is given by

$$t_d^\beta = \frac{L}{V}\left(1 - \frac{V}{\beta}\cos\theta\right).$$

For most earthquakes, it has been found that V is less than β but is very close to it. Therefore,

$$t_d^\alpha - t_d^\beta = \frac{L}{\beta}\left(1 - \frac{\beta}{\alpha}\right)\cos\theta \simeq (0.42\,L/\beta)\cos\theta.$$

For major earthquakes, this difference could be as much as 1 min.

In the case of a vertical strike slip fault, the horizontal radiation pattern is given by

$$F = \sin 2\phi,$$

where ϕ is the azimuthal angle. Equation (5) then becomes

$$u^P = \frac{P_0 V}{12\pi\beta LR_0} (\beta/\alpha)^3 \frac{\sin 2\phi}{1 - (V/\alpha)\cos\phi} \times \left[g(t_\alpha) - g(t_\alpha - t_d^\alpha)\right]. \quad (6)$$

Thus the radiation pattern for P waves due to a finite moving source is given by the factor

$$\frac{\sin 2\phi}{1 - (V/\alpha)\cos\phi}, \quad (7)$$

instead of the usual $\sin 2\phi$ for a point source. Similarly, for S waves from a finite moving source, the radiation pattern is given by

$$\frac{\cos 2\phi}{1 - (V/\alpha)\cos\phi} \quad (8)$$

These are shown in Figure 3.

Spectral displacements

Assuming

$$U(s, t) = f(s)\, g(t), \quad (9)$$

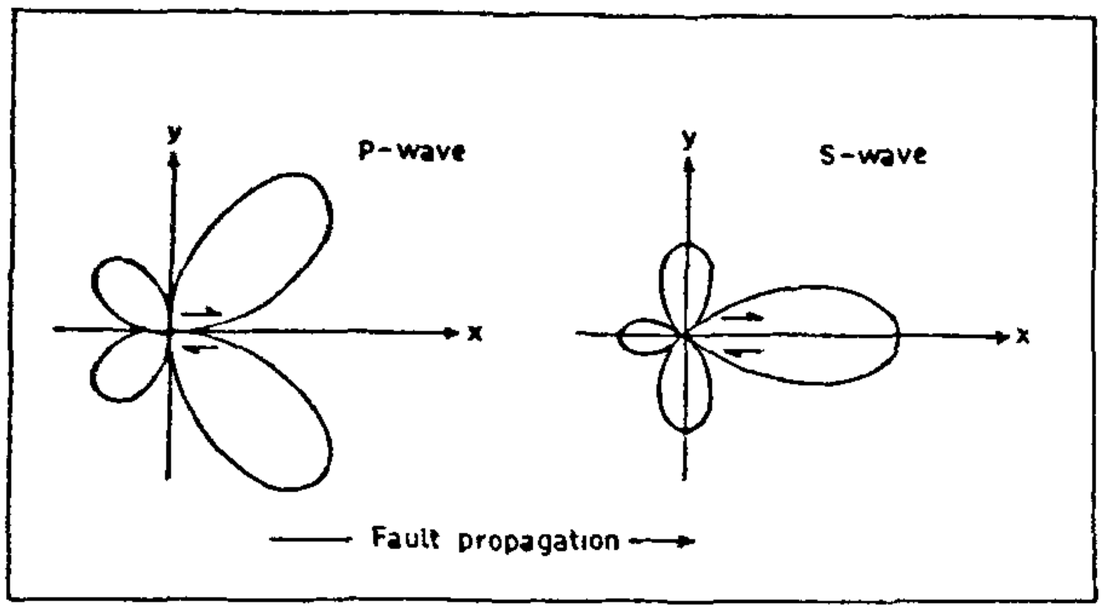

Figure 3. The horizontal radiation patterns of P and S waves from a finite moving strike-slip dislocation.

equation (3) becomes

$$u^P = \frac{W}{12\pi\beta}(\beta/\alpha)^3 \frac{F}{R_0}\int_0^L f(s) \times \dot{g}\left[t - \frac{R_0}{\alpha} - \frac{s}{V}[1-(V/\alpha)\cos\theta]\right] ds. \quad (10)$$

Taking Fourier transform, we get

$$u^P(\omega) = \frac{W}{12\pi\beta}(\beta/\alpha)^3 \frac{F}{R_0}[i\omega g(\omega)] \exp(-ik_\alpha R_0) \times \int_0^L f(s) \exp(-i\omega_\alpha s/V)\, ds, \quad (11)$$

where $g(\omega)$ is the Fourier transform of $g(t)$ and

$$k_\alpha = \omega/\alpha, \quad \omega_\alpha = \omega[1-(V/\alpha)\cos\theta]. \quad (12)$$

If $f(s) = U_0$, equation (11) yields

$$u^P(\omega) = \frac{WU_0}{12\pi\beta}(\beta/\alpha)^3 \frac{F}{R_0}[i\omega g(\omega)] \times \exp(-ik_\alpha R_0)\int_0^L \exp(-i\omega_\alpha s/V)\, ds$$

$$= \frac{P_0}{12\pi\beta}(\beta/\alpha)^3 \frac{F}{R_0}[i\omega g(\omega)] \times (\sin X_\alpha/X_\alpha)\exp(-ik_\alpha R_0 - iX_\alpha), \quad (13)$$

where

$$X_\alpha = \frac{L\omega_\alpha}{2V} = \frac{L\omega}{2V}[1-(V/\alpha)\cos\theta]. \quad (14)$$

The factor $(\sin X_\alpha/X_\alpha)\exp(-iX_\alpha)$ is a first-order correction for the finiteness of the source and its motion. If $L = 0$, $X_\alpha = 0$, and this factor is unity. This factor affects both the amplitude and the phase. An observer will notice a phase retardation X_α and an amplitude modulation $\sin X_\alpha/X_\alpha$ which is a function of the frequency ω, the polar angle θ, the rupture duration L/V and the Mach number V/α. The P-wave amplitude vanishes for the values of ω that make X_α an integral multiple of π (Figure 4). This is the condition for the destructive interference of P waves at the point of observation.

In equation (13), the frequency dependence of $u^P(\omega)$ is through the factor

$$A(\omega) = [i\omega g(\omega)](\sin X_\alpha/X_\alpha)\exp(-iX_\alpha - ik_\alpha R_0)$$

with modulus

$$|A(\omega)| = \omega|g(\omega)||\sin X_\alpha/X_\alpha|.$$

At the high frequency end of the spectrum the dependence on ω is roughly that of $|g(\omega)|$. In contrast, at low frequencies, $\sin X_\alpha/X_\alpha \simeq 1$, and the dependence is roughly like $\omega|g(\omega)|$.

Two source time-functions need special mention. Ben-Menahem and Toksoz[11] used the exponential buildup time-function

$$g(t) = 0 \quad t < 0,$$
$$= 1 - e^{-t/T}, \quad t > 0, \quad (15)$$

for which

$$g(\omega) = \frac{1}{i\omega(1+i\omega T)}. \quad (16)$$

Haskell[4, 12] used a ramp function

$$g(t) = 0 \quad t < 0,$$
$$= t/T \quad 0 < t < T,$$
$$= 1 \quad t > 0, \quad (17)$$

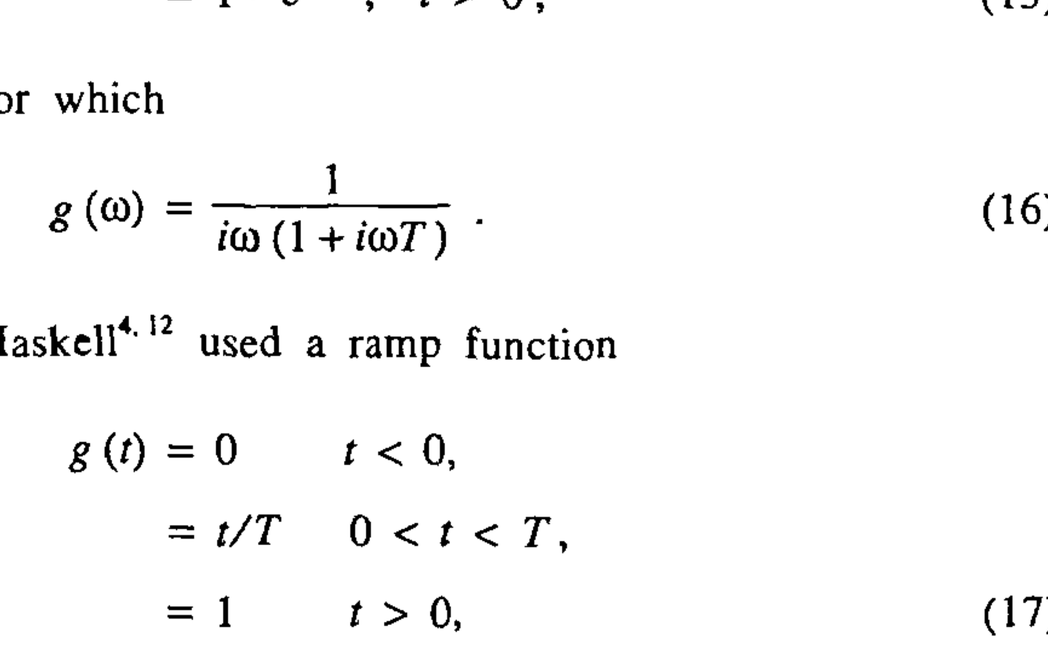

Figure 4. The finiteness factor in the spectrum (after Aki and Richards, 1980)

for which

$$g(\omega) = \frac{1}{i\omega} \cdot \frac{\sin(\omega T/2)}{\omega T/2} \cdot \exp(-i\omega T/2). \quad (18)$$

The parameter T is known as rise time. In both cases, for low frequencies, as ω tends to zero, the spectral amplitude tends to a constant value. At high frequencies, the spectral amplitude varies as ω^{-2}. The frequency at the intersection of the low- and high-frequency asymptotes in the spectrum is known as corner frequency (Figure 5). It has been found that the corner frequency is inversely proportional to the dimensions of the source.

According to Brune[13], the radius of a circular fracture is related to the corner frequency of the spectrum of S waves by

$$\omega_c = 2.21\ \beta/r. \quad (19)$$

Savage[14] calculated the corner frequencies for P and S waves for a model of a rectangular bilateral fault of length L, width W and a rupture velocity $V = 0.9\beta$, with the following results

$$\omega_c^P = 1.7\,\alpha/\sqrt{LW},$$

$$\omega_c^S = 3.8\,\beta/\sqrt{LW}. \quad (20)$$

From Brune's result, taking $\pi r^2 = LW$, we have

$$\omega_c = 2.21\,\beta/r = 2.21\,\beta/\sqrt{LW/\pi} = 3.9\,\beta/\sqrt{LW}, \quad (21)$$

which agrees well with the above result of Savage for S waves.

The complete process of fracture propagation includes the description of its nucleation, spreading and stopping. Let the slip be specified such that it comes to stop when the limit of the fault is reached. Then the phase generated by the stopping of the rupture is called the stopping phase. The relative importance of the initiating and stopping phases depends upon the model assumed for the slip.

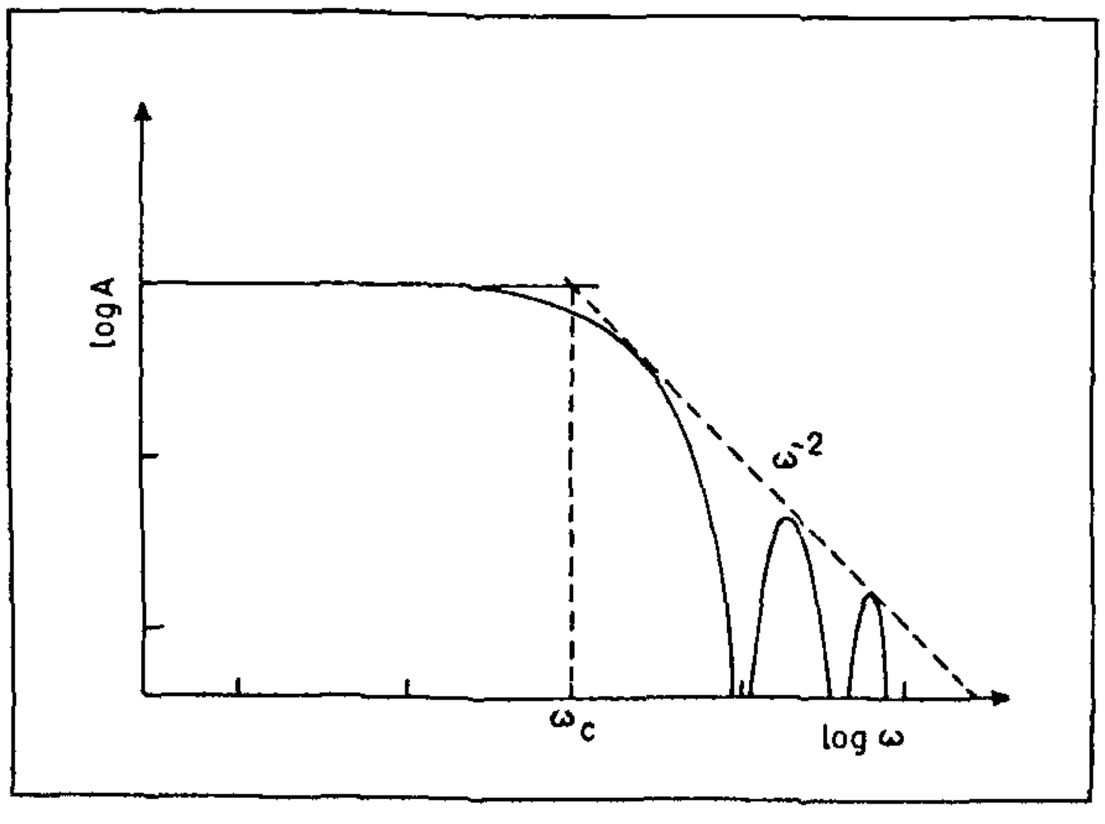

Figure 5. The corner frequency

Displacement near a fault

The displacement field due to a finite fault S with slip U is given by[10]

$$u_i(x, t) = \frac{1}{4\pi} \iint_S \frac{1}{\beta R}\left[F_1\ \dot{U}\left(t - \frac{R}{\beta}\right) + \left(\frac{\beta}{\alpha}\right)^3 F_2\,\dot{U}\left(t - \frac{R}{\alpha}\right)\right] dS(y) + \frac{1}{4\pi} \iint_S \frac{1}{R^2}\left[F_3 \int_{\beta/\alpha}^{1} U\left(t - \frac{sR}{\beta}\right) s\ ds + F_4\,U\left(t - \frac{R}{\beta}\right) + \left(\frac{\beta}{\alpha}\right)^2 F_5\, U\left(t - \frac{R}{\alpha}\right)\right] dS(y), \quad (22)$$

where $x(x_1, x_2, x_3)$ = position vector of the receiver, $y(y_1, y_2, y_3)$ = position vector of the point of integration on the fault, $U = dU/dt$ = slip velocity, and $R = |x - y|$. The functions F_i depend upon the fault normal n, the slip direction e and the direction cosines $\gamma_i = (x_i - y_i)/R$.

Each of the terms under the surface integral has a simple form, attenuating as a certain negative power of distance from the source. The terms attenuating as R^{-1} are the far-field terms and the terms attenuating as R^{-2} are the near-field terms. The wave form of each term can be easily calculated for a given slip function $U(y; t)$. It is difficult, however, to make a general statement on the total displacement because, at short distances, these terms arrive almost simultaneously, often cancelling each other and the behaviour of the sum of all the terms is quite unpredictable from separate consideration of each individual term. This is especially true for motion close to the fault, because each term tends to infinity as $R \to 0$, although physically we expect the sum of all the terms to be finite. Therefore, near a fault, total seismograms consisting of the near-field as well as the far-field terms must be computed for comparison with observations.

Theoretical seismogram can be calculated by direct numerical integration of equation (22). For numerical

integration, we replace the integral by a summation over grid points. We assume that the dislocation propagates along the length L of a rectangular fault ($L \times W$) with rupture velocity V; then the Ben-Menahem transfer function for an element $\Delta L \times \Delta W$ (Figure 6) of the fault is

$$(\sin X_c / X_c)\ \exp(-iX_c)$$

where

$$X_c = \frac{\Delta L \omega}{2V}\left(1 - \frac{V}{c}\cos\theta\right)$$

and c is either α or β. We can then sum these terms over all the grid points. The time domain solution for a given slip function can be synthesized from the spectral solution. The grid interval must be taken to be sufficiently small so that the far-field approximation used in the derivation of the Ben-Menahem transfer function is valid. Therefore, for points of the fault close to the point of observation, the grid interval will be much smaller than for points farther away. Furthermore, the grid interval must be much smaller than cT, where T is the rise time.

Figure 7 shows the perpendicular component of the horizontal displacement (calculated from the original acceleration record by numerical integration) observed by a strong-motion seismogram located only 80 m away from the San-Andreas fault during the Parkfield, California earthquake of 28 June 1966. It was shown by Aki[3] and Haskell[4] that the observed motion is precisely what is expected for a right-lateral strike-slip fault. Figure 8 shows the theoretical displacement seismogram synthesized by Aki for a propagating fault. In order to calculate a theoretical seismogram, the details of the rupture process must be specified. Aki and Haskell used a simple five-parameter model, now called Haskell's model, in which a uniform slip U takes place over a rectangular fault with width W and length L. The rupture propagates along the length with a constant velocity V. The slip at any point on the fault starts to increase linearly with time at the arrival of the rupture front, and stops when the amount of slip reaches U. The time required to complete the slip is the rise time T, and is assumed to be the same at every point. Thus, Haskell's model is described completely by five parameters: length, width, final slip, rupture velocity and rise time. Aki[3] obtained an excellent agreement between the observed and the theoretical seismograms for the Parkfield earthquake and concluded that at very short distances: (i) the dislocation (slip) is the only important source parameter that controls the seismic motion; (ii) the rupture velocity is a significant but not dominant factor; (iii) other source parameters such as the fault length and depth show negligible effect on the motion.

The kinematical models of the source mechanism of earthquakes assume a certain function of space and time for the slip $U(y; t)$ over the fault area. The form of the fault surface and the rupture velocity must also be assumed in the model. From the physical point of view, the kinematical models have many shortcomings, e.g. near the edge of the fault the stress drop is infinite.

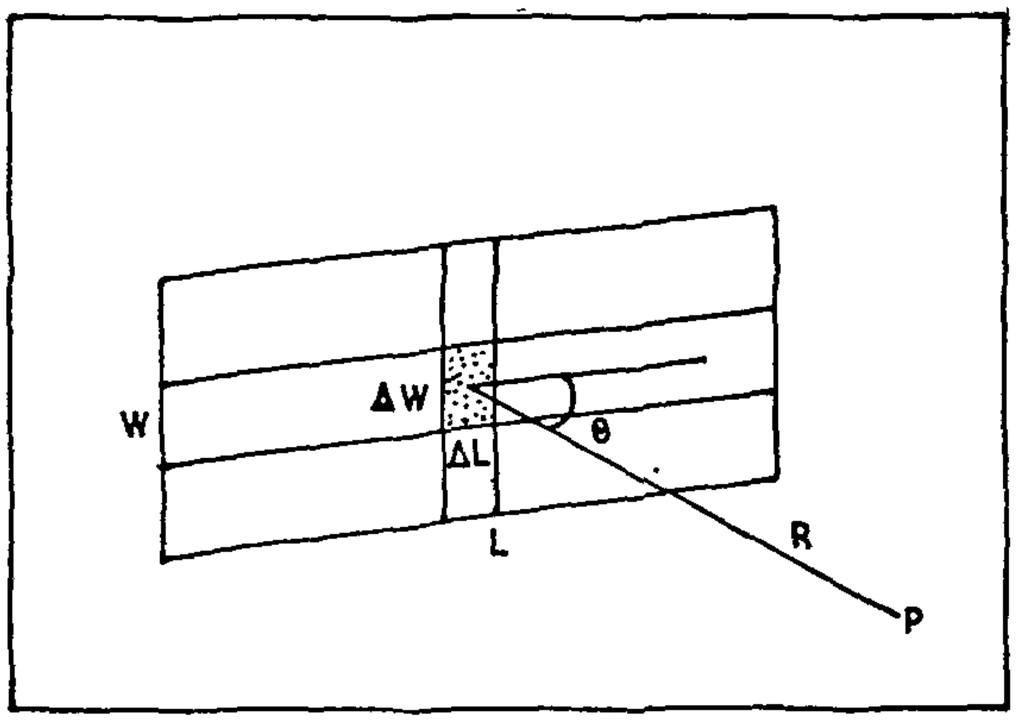

Figure 6. Grid points selected for numerical integration of equation (22).

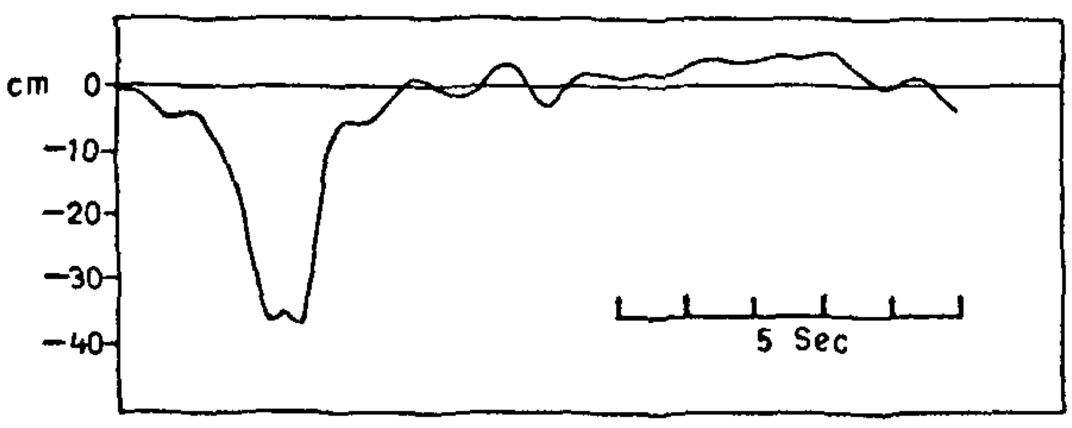

Figure 7. The displacement observed at 80 m from the San Andreas fault in the direction perpendicular to the fault trace during the 1966 Parkfield earthquake (after Aki, 1968).

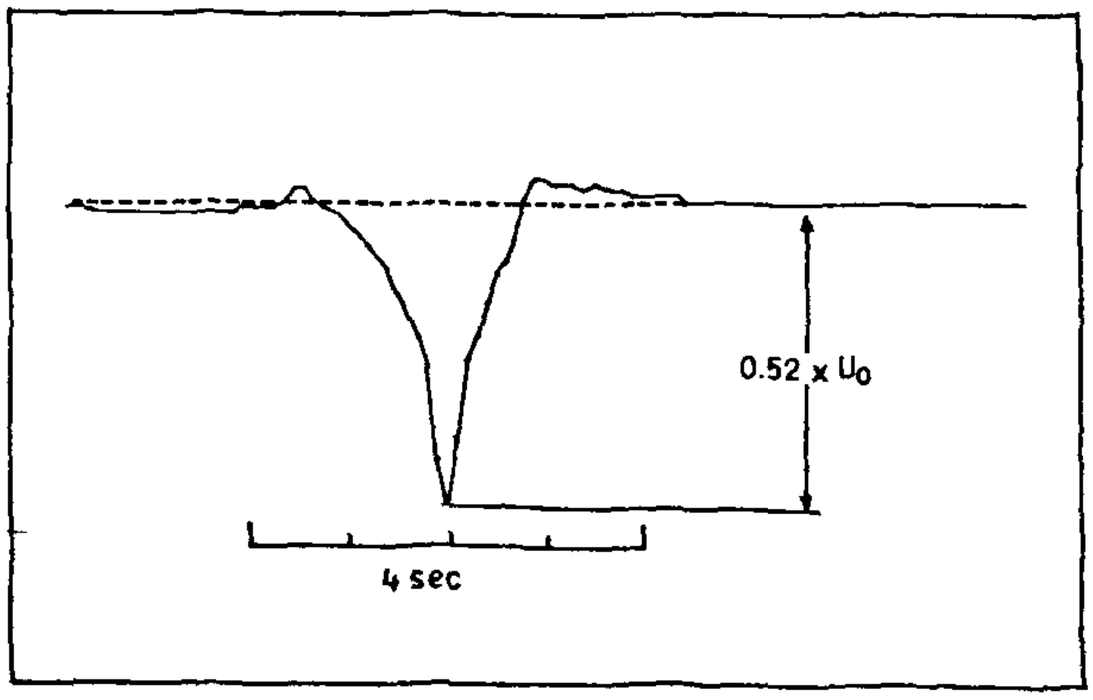

Figure 8. Synthetic displacement corresponding to the observation shown in Figure 7 for a right-lateral strike-slip fault propagating with rupture velocity 2.2 km/s (after Aki, 1968).

To obtain more physically realistic models, one must proceed to establish dynamic models in which the slip is one of the unknowns derived from the state of stress and the strength of the material at the source region. The general problem of dynamic models is based on the idea of crack formation and propagation in a prestressed medium. A discussion of the dynamic models of earthquake source mechanism is beyond the scope of this paper (see e.g. refs 15 and 16).

1. Maruyama, T., *Bull. Earthq. Res. Inst*, *Tokyo Univ.*, 1963, **41**, 467–486.
2. Burridge, R. and Knopoff, L., *Bull. Seismol. Soc. Am.*, 1964, **54**, 1875–1888.
3. Aki, K., *J. Geophys. Res.*, 1968, **73**, 5359–5376.
4. Haskell, N. A., *Bull. Seismol. Soc. Am.*, 1969, **59**, 865–908.
5 Kawasaki, I., Suzuki, Y. and Sato, R, *J. Phys. Earth*, 1975, **23**, 43–61.
6. Heaton, T. H. and Helmberger, D. V, *Bull. Seismol Soc. Am.*, 1977, **67**, 315–330.
7. Ben-Menahem, A, *Bull Seismol. Soc. Am.*, 1961, **51**, 401–435.
8. Ben-Menahem, A., *J. Geophys. Res.*, 1962, **67**, 345–350.
9. Ben-Menahem, A., *J. Phys. Earth*, 1986, **34**, 297–334.
10 Ben-Menahem, A. and Singh, S. J., *Seismic Waves and Sources*, Springer, New York, 1981.
11. Ben-Menahem, A. and Toksoz, M. N., *J. Geophys. Res.*, 1963, **68**, 5207–5222.
12. Haskell, N. A., *Bull. Seismol. Soc. Am.*, 1964, **54**, 1811–1841
13. Brune, J. N., *J Geophys. Res.*, 1970, **75**, 4997–5009.
14. Savage, J. C, *J. Geophys. Res.*, 1972, **77**, 3788–3795.
15. Aki, K. and Richards, P. G., *Quantitative Seismology Theory and Methods*, Freeman, San Francisco, 1980.
16. Kostrov, B V. and Das, S, *Principles of Earthquake Source Mechanism*, Cambridge University Press, Cambridge, 1988.

ACKNOWLEDGEMENTS I thank CSIR, New Delhi for financial support.

Uncertainties with strong motion earthquake parameters

N. C. Nigam
Department of Civil Engineering, Indian Institute of Technology, New Delhi 110 016, India

A large measure of uncertainty is associated with the earthquake ground motion. The characteristics of the earthquake ground motion are examined to identify the sources of uncertainties. Seismic risk analysis is presented to establish the distribution of peak ground motion parameters. Random process models of the earthquake ground motion are discussed.

Aseismic design of a structure involves prediction of the nature of ground motion at the site during the service life of the structure. This in turn requires: (i) identification of the potential sources of strong motion earthquakes; (ii) geometry of each source; (iii) magnitude, epicentral location and focal depth, and time history of occurrence of past earthquakes for each source; and (iv) attenuation laws.

A large measure of uncertainty is associated with each of the above factors. The cumulative effect of these uncertainties makes the earthquake-induced ground motion at a point, a time-dependent random process vector. In earthquake engineering, it is convenient to resolve this vector into three random processes—two along perpendicular directions in the horizontal plane and one vertical. The uncertainty in the earthquake-induced ground motion may, therefore, be represented to varying degree of completeness by: (i) ensemble of sample functions; (ii) hierarchy of joint probability distribution, or characteristic functions; (iii) envelope functions, and intensity moments[1]; (iv) spectral density functions and spectral moments[2], Fourier and response spectra; and (v) gross properties of ground motion components in terms of random variables, such as, peak values of ground acceleration, velocity and displacements, r.m.s. value, duration, spectral intensity, etc.

For long structures with a dimension significantly large as compared to the characteristic wavelengths in earthquake ground motion, the spatial randomness must also be considered and the ground motion must be modelled as a multi-parametered random process vector. This introduces additional uncertainties.

In this paper we consider the cumulative effect of uncertainties associated with various factors to establish the distribution, and other characteristics of ground motion at a point in terms of: (i) peak ground acceleration, velocity and displacement treated as random variables; and (ii) ground motion time-histories, treated as random processes. First, we consider the characteristics of the earthquake induced ground motion.